Deformation and Failure in Stochastic Fibrous Networks: Scale, Dimension and Application

A.M. Sastry, C.-W. Wang, L. Berhan
Department of Mechanical Engineering | Department of Biomedical Engineering
University of Michigan, Ann Arbor 48109-2125

Keywords: damage, electrochemical, failure, fiber, mechanics, multifunctional, network, percolation, stochastic

Abstract
There is an extensive literature on identification and analysis of representative volume elements (RVE's) in order to bound intrinsic materials properties in porous and nonporous solids. However, in such analyses there is often an implicit assumption made that solution of several large classes of linear scientific problems can be simultaneous achieved simply via a single solution of Laplace's equation for the domain. We find, however, that for an extremely technologically significant class of disordered fibrous/particular structures, the transport properties and the mechanical properties cannot simultaneously be found using a single field solution. Specifically, alterations in microstructure during loading of the material can produce different degrees of effects on mechanical load transfer and conductivity. The details of load transfer within stochastic, porous arrays are critical in understanding their likely properties, which we have shown to exhibit large variability. Nonetheless, through thoughtful use of stochastic finite element simulation, we are able to provide technologically useful guidance on material synthesis, construction, and estimations of lifetime in several key contexts. In doing so, we have addressed several mathematical issues of solution of field equations around singularities produced by phase contrast, boundary condition choice and material contrast, and geometric features inherent in fused structures. This work is a summary of some of our key findings on the subject, and suggests a roadmap for new areas of study, based both on our simulations and on our experiments on materials used in battery systems.

1. Introduction

We have extensively investigated both mechanical [1-5] and transport [4-8] properties of stochastic fibrous networks. Several examples of materials investigated are shown in Figs. 1 and 2. Critical features of these materials include 1) their low density, 2) irregular internal microstructure, 3) reliance on contact of sometimes dissimilar constituent particles in providing electrical conductivity and 4) their microstructural alteration in the presence of normal service loads.

In Fig. 1, microstructural evolution of an NiMH positive cell substrate is shown, in which a corrosion process results in microstructural changes (compare sketches of Figs. 3a and 3b for microstructural assumption). In Fig. 2, a negative plate of a commercial Li-ion cell is shown, wherein carbon particles of highly variable size and shape form a conductive, electrochemically active array. In both of these battery technologies, cells undergo internal mechanical loads during cycling, due to irreversible formation of lower-density side products (NiMH) and intercalation of carbons and gas formation (Li-ion), respectively.

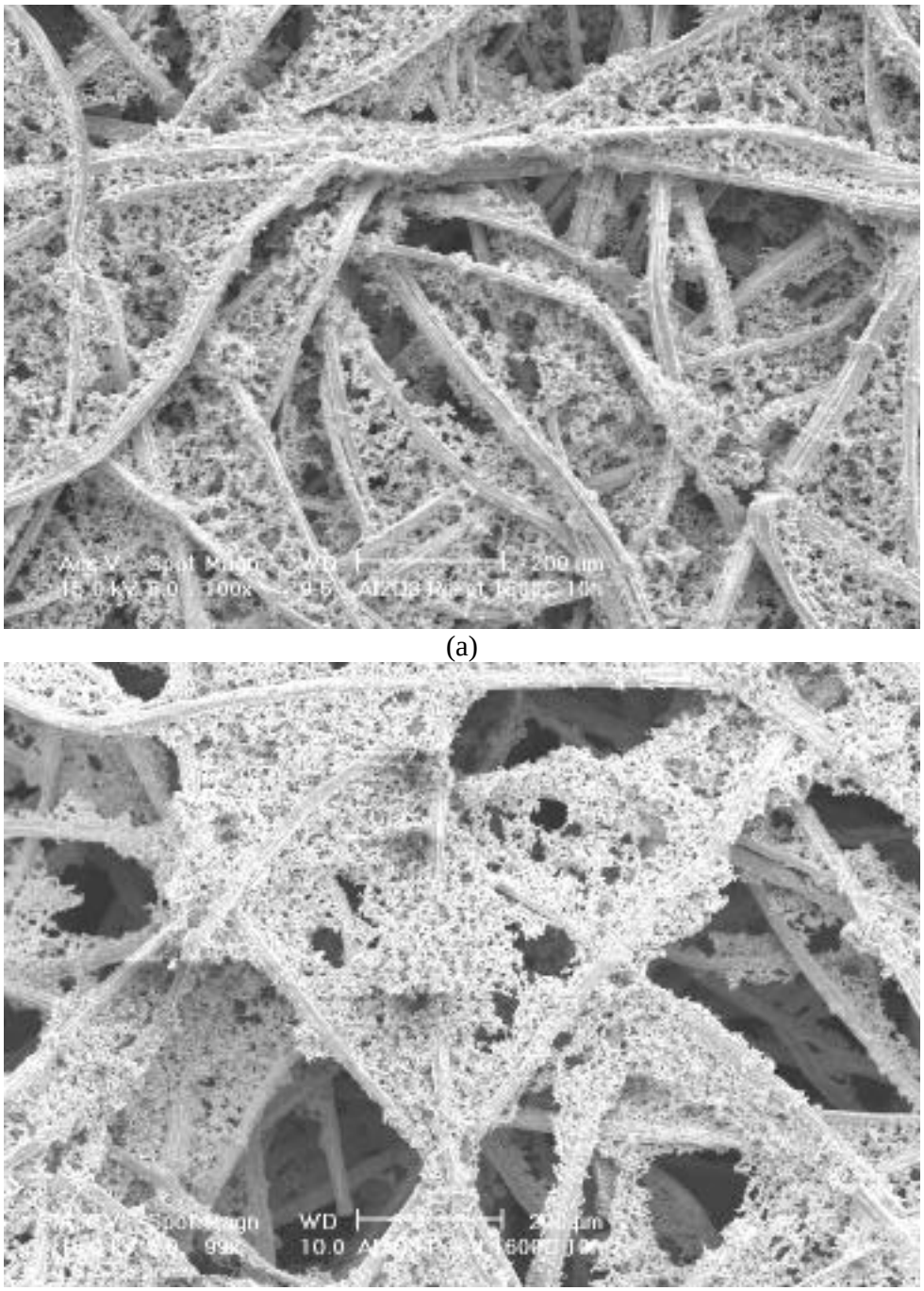

(a)

(b)

Figure 1. *Scanning electron micrographs of positive substrates in the (a) compressed to the post-cycled volume fraction (~10%), and (b) post-cycled (40 constant current cycles and 150% overcharge) condition*

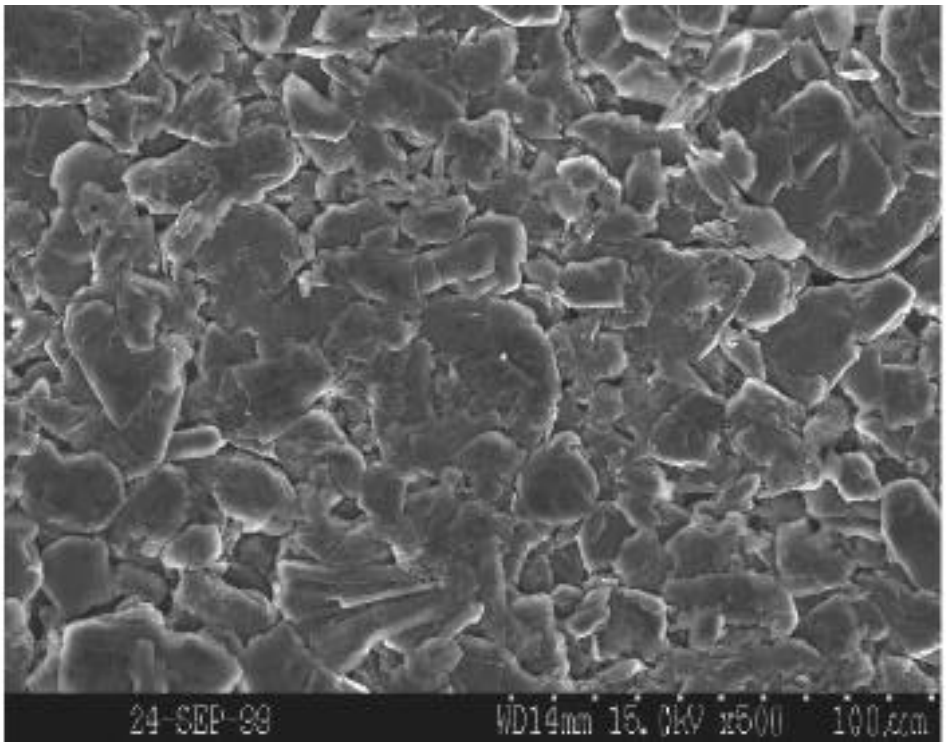

(a)

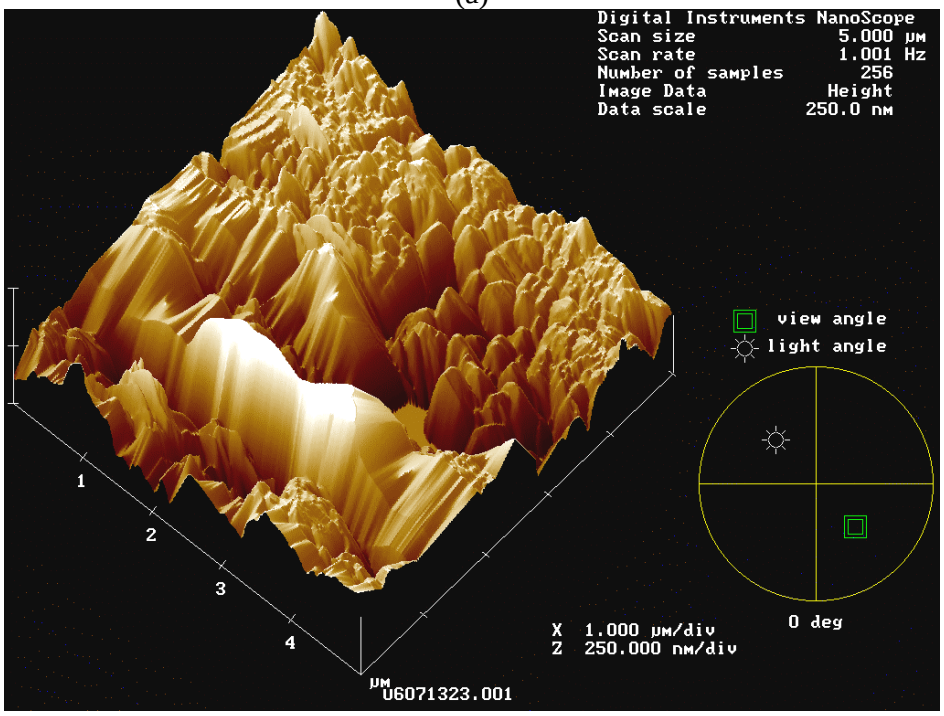

(b)

Figure 2. *(a) Scanning electron micrograph with 500x magnification, and (b) contacting atomic force microscope image of negative substrates of the Panasonic CGP30486 lithium-ion battery.*

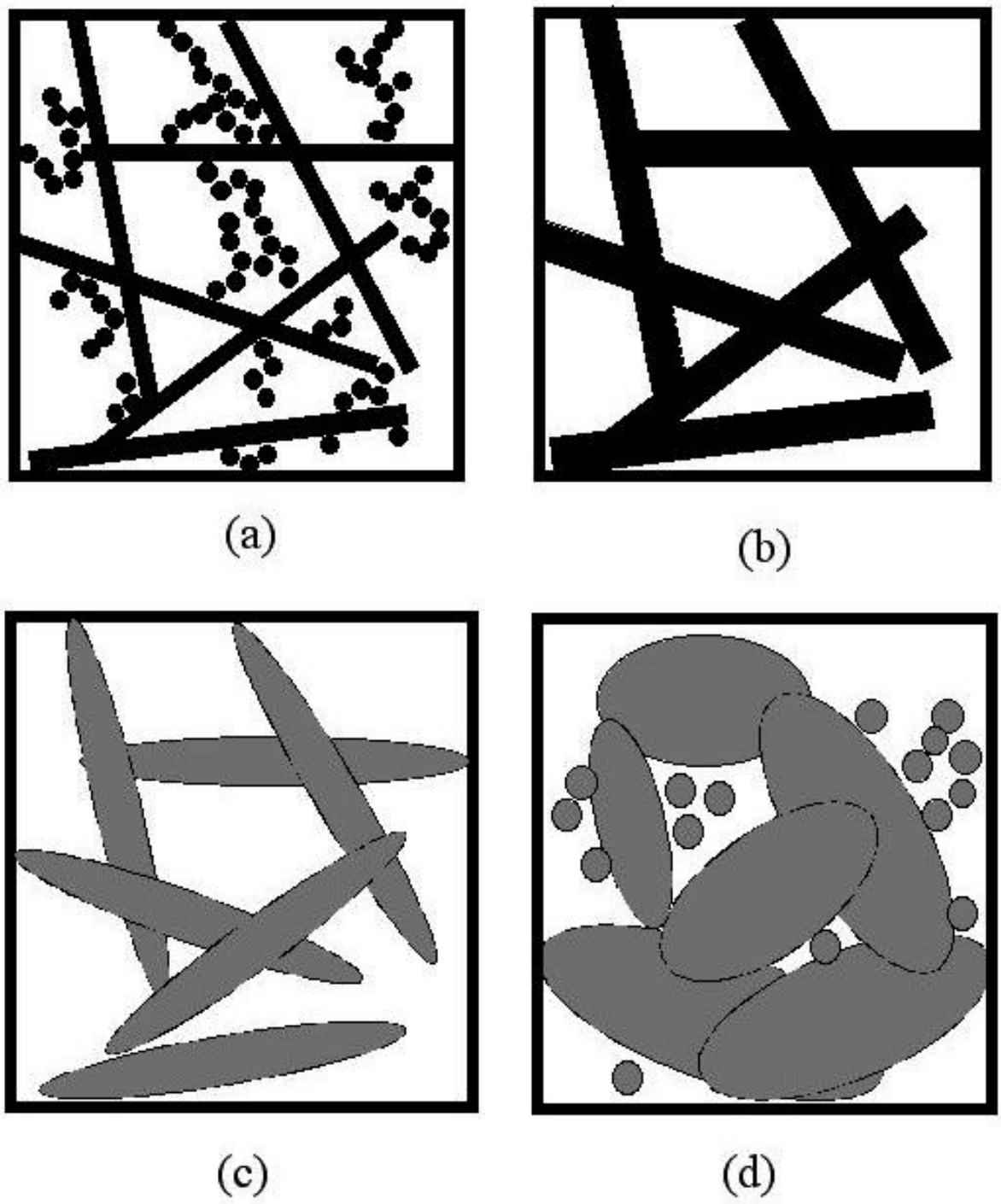

Figure 3. *Four possible representations for porous materials comprised of fibers and particles, including (a) beams representing fibers, with spherical particles, (b) 2D beams representing fibers, (c) 2D ellipses representing fibers and (d) ellipsoidal particles of varying aspect ratio, representing both fibers and particles.*

Beyond these battery technologies, there are of course a number of other examples of technologically and scientifically significant porous, fibrous/particulate materials. A few of these include paper, biomaterials (e.g. trabecular bone, collagen networks), filters, fiberboard, etc. The continued drive toward analysis of ever smaller-scale materials, and the demonstrated applicability of some aspects of Newtonian mechanics in polymer networks, suggest that such analysis of stochastic arrays offers much for problems of high future interest. Additionally, the approaches taken in the past, including closed-form percolation models [10-16], will likely be supplanted by more accurate but previously impractical, large-scale (i.e. real-scale or nearly real-scale) simulations of more realistic microstructure.

Much of this extensive literature on indentification and analysis of RVE's in order to bound intrinsic materials properties hinges on an implicit assumption that solution of several large classes of linear scientific problems can be simultaneous achieved simply via solution of Laplace's equation for the domain. For an excellent review on a great deal of the classical work, see Meredith and Tobias [17]. Our simulations reveal, however, that for the extremely technologically significant class of disordered fibrous/particular structures studied, the transport properties and the mechanical properties cannot simultaneously be found using a single field solution. Specifically, alterations in microstructure during loading of the material can produce different degrees of effect on mechanical load transfer and conductivity.

Our stochastic approach has centered on generation of, and simulations of response of realistic microstructures, described by statistical distributions obtained from image analysis of real materials. In conduction modeling, we have taken two main approaches, which are described presently. In mechanics modeling, we have undertaken modeling of both connecting particles' response and the behavior of internal joints, or synapses. More recently, we have considered fully three-dimensional modeling.

2. Representations of Microstructure and Transport Analysis

Strategies for representation of microstructure (several examples of which are shown in Fig. 3) depend upon strategies for solution of governing equations in the domain of interest. Combinations of fibers and particles in a stochastic array (Fig. 3a) may be considered, for example, as only an array of fibers (Fig. 3b), if the conduction problem is to be solved, and the particle phase can be considered unimportant (i.e. is not of sufficient volume fraction to form an interpenetrating percolated network). The same array might be conceived of as an array of narrow ellipses (Fig. 3c) if one wished to solve a set of field equations in the array, and thus wished to reduce the presence and order of the attendant geometric singularities produced by sharp corners defining particle

boundaries (though not intersection boundaries). Note that this approach still requires consideration of these singularities [6] but strategic choice of simulation type can drastically reduce both the number of iterations required in solution, and the convergence of the solution [*ibid.*]. Consideration of particulate networks with somewhat smaller particle aspect ratios (e.g. Fig. 3d) can be accomplished using this approach, offering a convenient mathematical description of particles ranging from fiber-like to spheroidal; this advantage becomes evident in analysis of structures with a widely-varying distributions of particle shape which one would like to define with a single set of parameters.

Two approaches used in our transport work are shown schematically in the flowchart of Fig. 4. We have carried out conduction and mechanics simulations of generated microstructures using both the 1D fiber-generating approach on the left of Fig. 4 [1-5; 7], and conduction simulations using the field-of-ellipses approach on the right [6]. Our general approach is most clearly illustrated by demonstration. Two sample fiber networks are shown in Fig. 5. In Figs. 5a and 5b, and Figs. 5c and 5d, original and reduced networks are shown for volume fractions of 20% and 70%, respectively. The basic scheme is as described in Fig. 4, namely, fibers of statistically-described shape and orientation are placed in a simulation "window," whereupon periodicity is enforced (i.e. "ends" extending beyond the window are reflected within) and truncation of free ends in the network is performed. This last step is an efficiency possible with analysis of porous, rather than matrix-filled materials; the ends in porous materials provide negligible contribution to conductivity, and little contribution to mechanical loads (if mass is neglected and large-deformation impingement of fiber ends on fiber struts is not considered). In simulations of fields of ellipses, the last step is not performed, since this approach assumes that a full-field solution is desired, in part to address the effects of finite phase contrast.

Two arrays of fields-of-ellipses are shown in Fig. 6. In contrast with a 1D fiber assumption, here we solve the field equations for the array rather than use a circuit analysis (assuming fibers comprise 1D resistors) in conduction analysis. Use of higher aspect ratio elliptical particles rather than circular particles dramatically improves the conductivity of the array in this example; here we see a single example of the advantage of higher aspect ratio in producing percolated networks at lower volume fraction and overall higher conductivities, with no mass penalty.

Scale dependency in simulation size has been explored for both types of networks in terms of conductivity [3,4,6,7]; we have found generally that classical reliance on closed-form percolation models does not sufficiently capture or characterize variability in networks, but that simulation of real microstructures within an order of magnitude of the actual structure produces excellent predictive capability of conductivity, even when tracking morphology changes in materials [3,4,7].

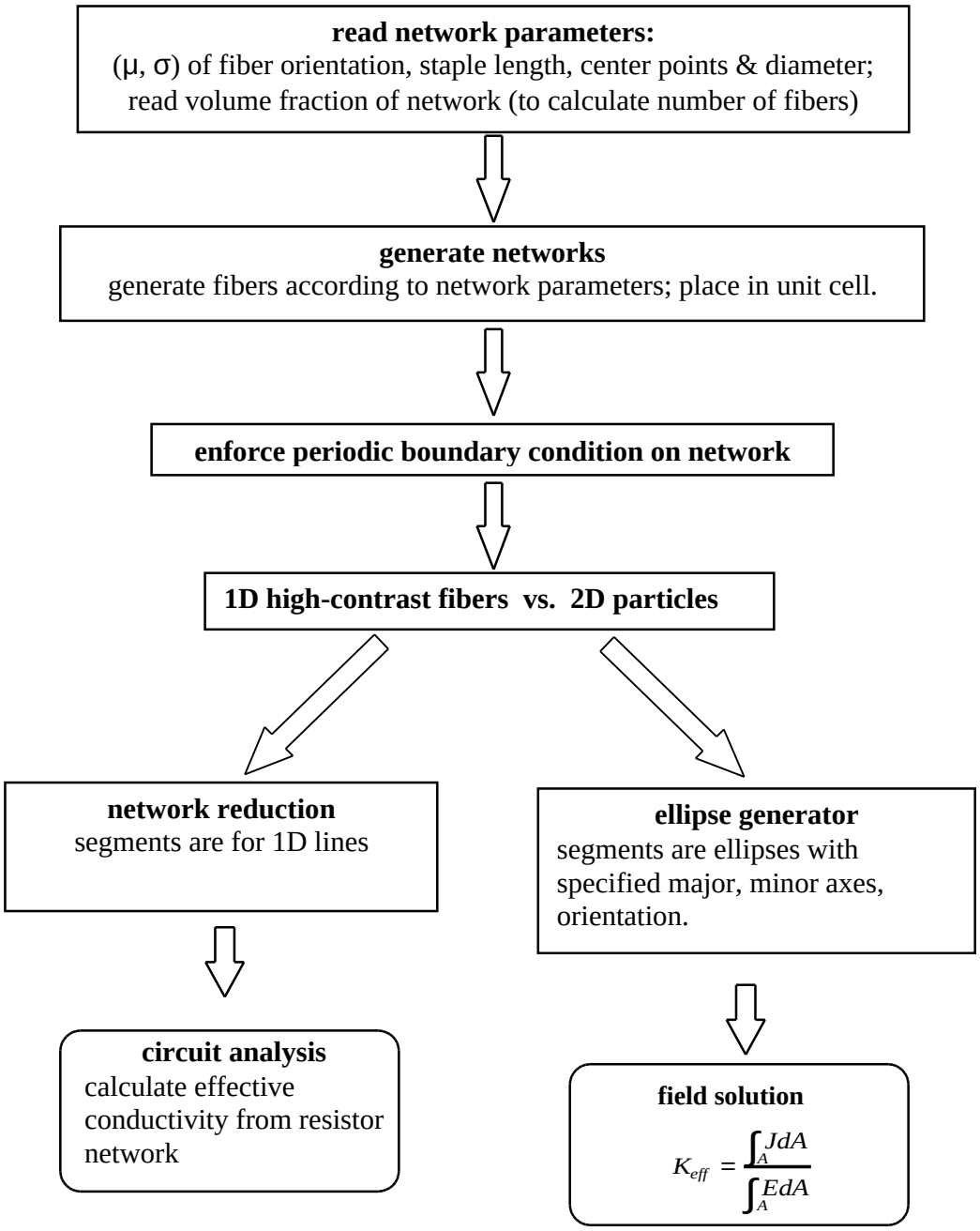

Figure 4*: Flow chart of network generation for the two approaches described.*

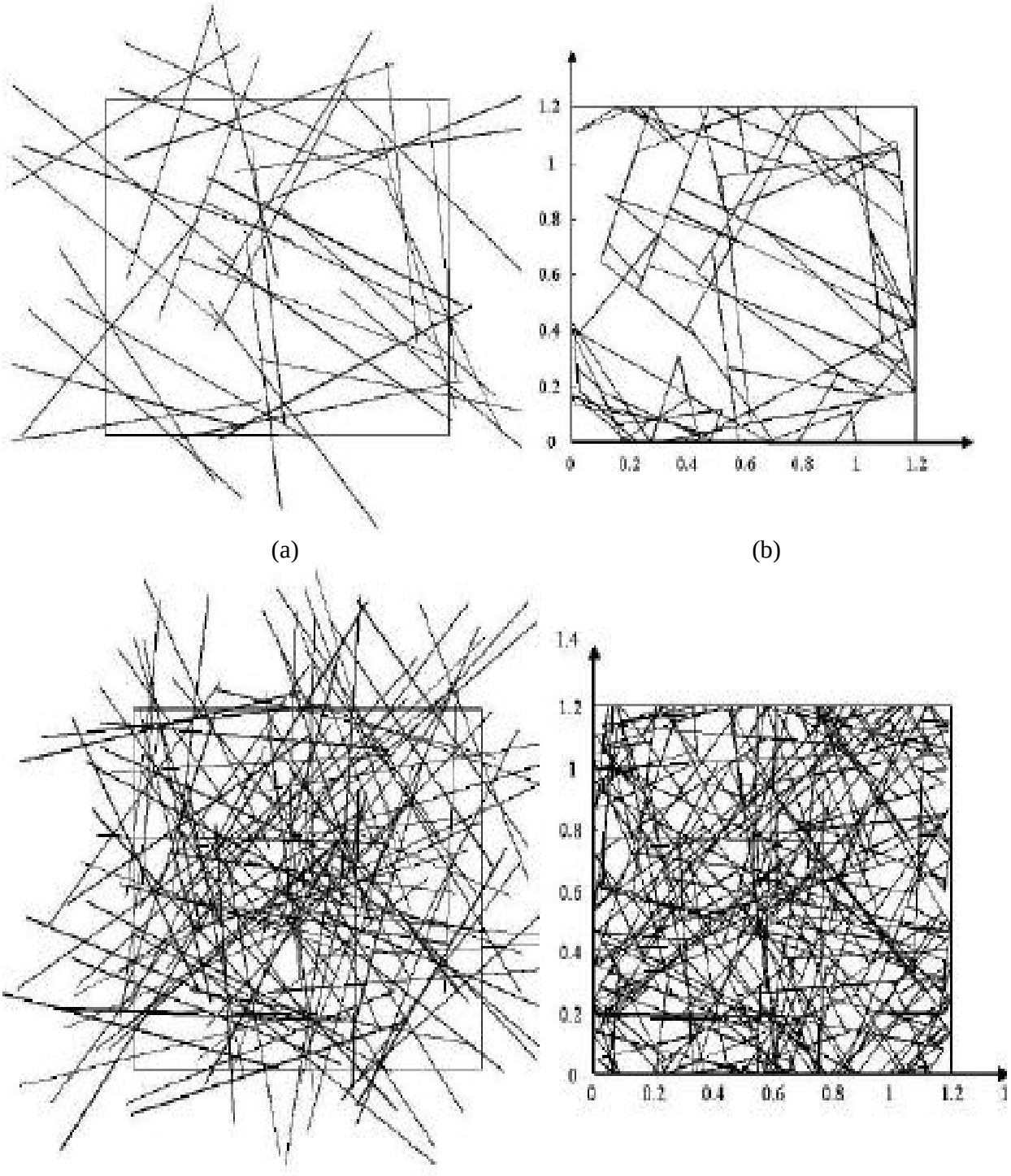

Figure 5. *Sample networks.In (a) and (b), a 20% initial volume fraction network is shown (a) before reduction and (b) after reduction. In (b) and (c), a 70% initial volume fraction network is shown (c) before reduction and (d) after reduction. Networks are comprised of fibers with diameter 0.01 and aspect ratio 100, with dimensions of networks as shown on the plots.*

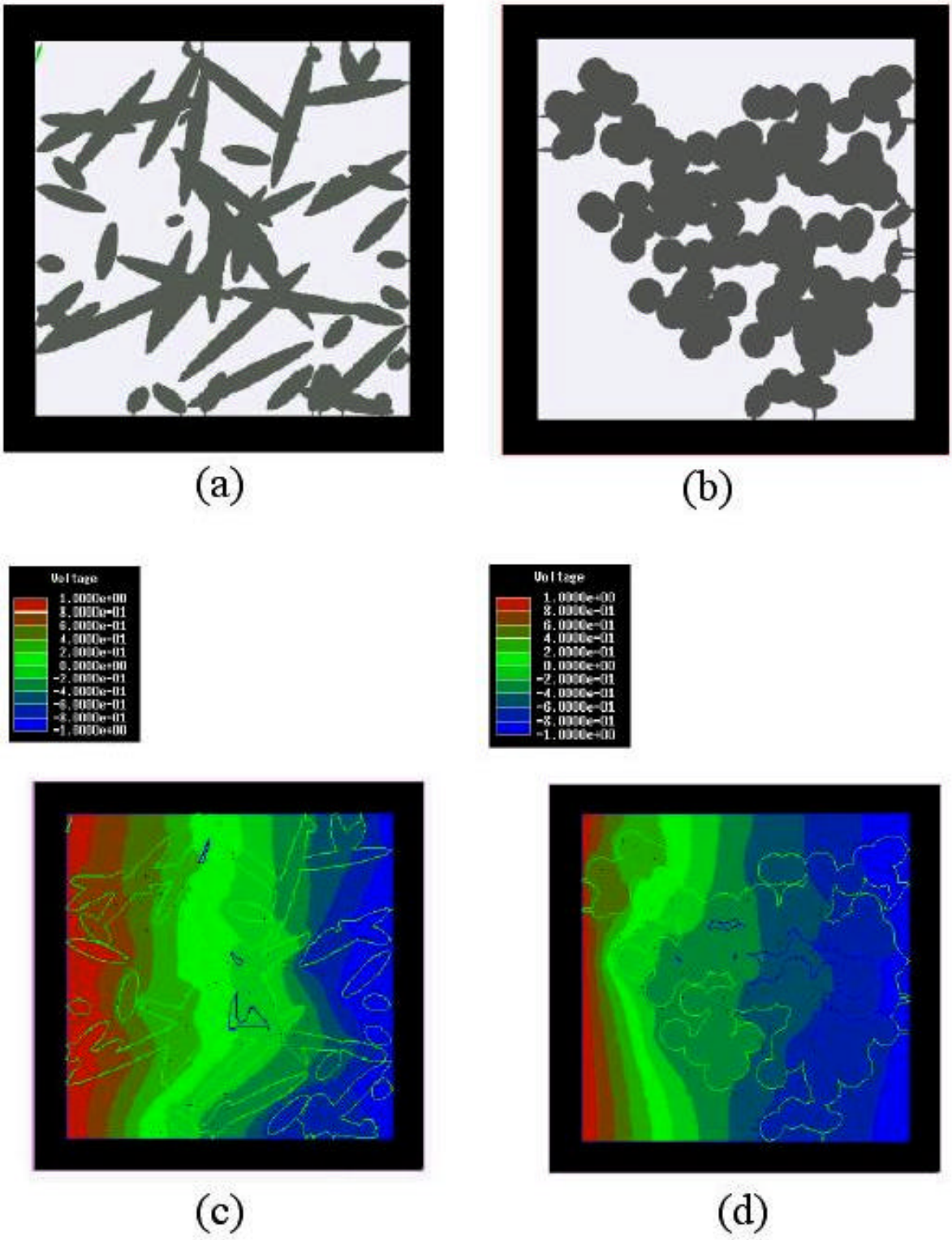

Figure 6. *Networks in a unit cell (original volume fraction ≈ 50%) comprised of (a) ellipses with uniformly distributed major axis length (average length = 0.3), and fixed minor axis length 0.05, and (b) circles with diameter 0.1. Images (c) and (d) are voltage contours for fields (a) and (b) with boundary conditions prescribed as 1.0V at the left edge and -1.0V at the right edge and a ratio of particle conductivity to matrix conductivity of 50.Resulting normalized effective conductivities for there arrays arrays, $K_{effective}/K_{fiber}$,are (a) 0.0708, and (b)0.0 236, respectively.*

3. Mechanics Analyses: Mechanisms and Scale-Dependence

Our overall strategy in modeling the mechanics of stochastic fiber/particulate structures has focused on three aspects of porous networks: first, simulation of 2D fibrous, connecting "struts" in these materials have been considered; second, the joints within these 2D arrays were considered (as having some compliance by placement of a torsion spring at their juncture); and third, fully 3D fibers and fiber/particle interconnects have been considered. A strategy of separation of the elements for analysis of a porous network is shown in Fig. 7. The sometimes-porous interconnects can be considered separately from the deformation of the fibrous elements via either insertion of the aforementioned torsion spring (of some scaled compliance) at the interconnect, shown in Fig. 8, or via definition of some zone of compliance at the interconnect if the connecting region is relatively large compared with the fiber struts, as shown in Fig. 9. Solutions for these models, for both two-beam assemblies and for complete networks, has been described previously by the authors [1-3]. Briefly (following [1]), the governing equations for torsion-spring bonded Timoshenko beams are

$$\begin{aligned} EA\frac{d^2u}{dx^2} &= 0 \\ EI\frac{d^2\psi}{dx^2} - GAKs\left(\psi + \frac{dv}{dx}\right) &= 0 \\ GAKs\frac{d}{dx}\left(\psi + \frac{dv}{dx}\right) &= 0 \end{aligned} \tag{1}$$

where application of the boundary conditions

$$\text{at } x = 0 \rightarrow \begin{cases} EA\left(\frac{du}{dx}\right) = -F_1 & \text{or} \quad u = \text{constant} \\ EI\left(\frac{d\psi}{dx}\right) - K_1\left(\frac{dv}{dx} + \psi - \alpha_1\right) = Q_1 & \text{or} \quad \psi = \text{constant} \\ GAKs\left(\psi + \frac{dv}{dx}\right) = -S_1 & \text{or} \quad v = \text{constant} \end{cases} \tag{2}$$

$$\text{at } x = L \rightarrow \begin{cases} EA\frac{du}{dx} = F_2 & \text{or} \quad u = \text{constant} \\ EI\left(\frac{d\psi}{dx}\right) + K_2\left(\frac{dv}{dx} + \psi - \alpha_2\right) = Q_2 & \text{or} \quad \psi = \text{constant} \\ GAKs\left(\psi + \frac{dv}{dx}\right) = S_2 & \text{or} \quad v = \text{constant} \end{cases}$$

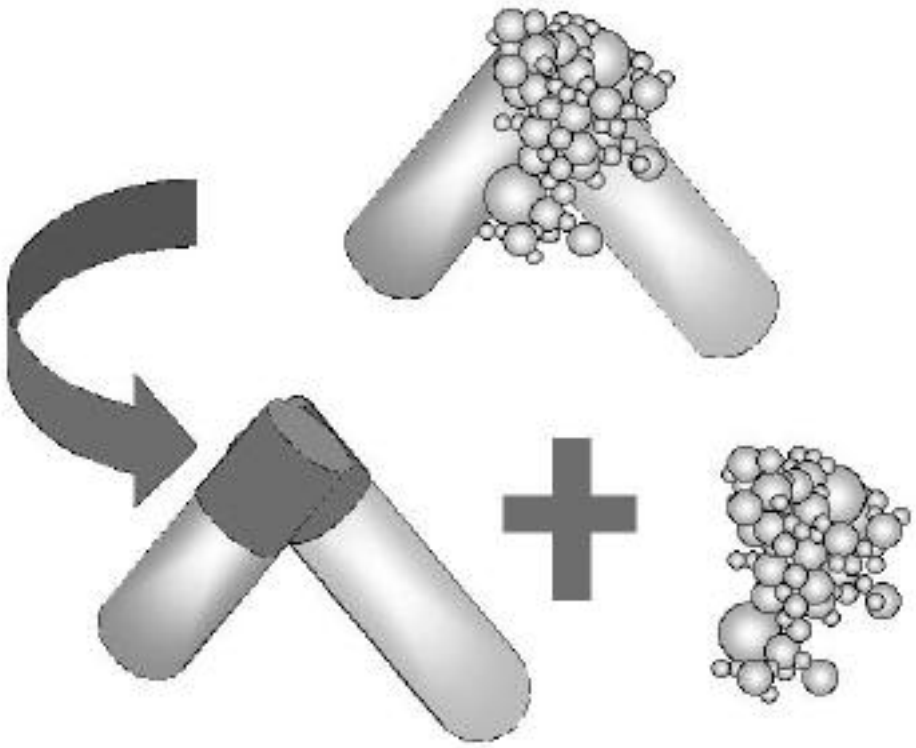

Figure 7. Strategy of separation of analysis of interconnecting beams from porous interconnects.

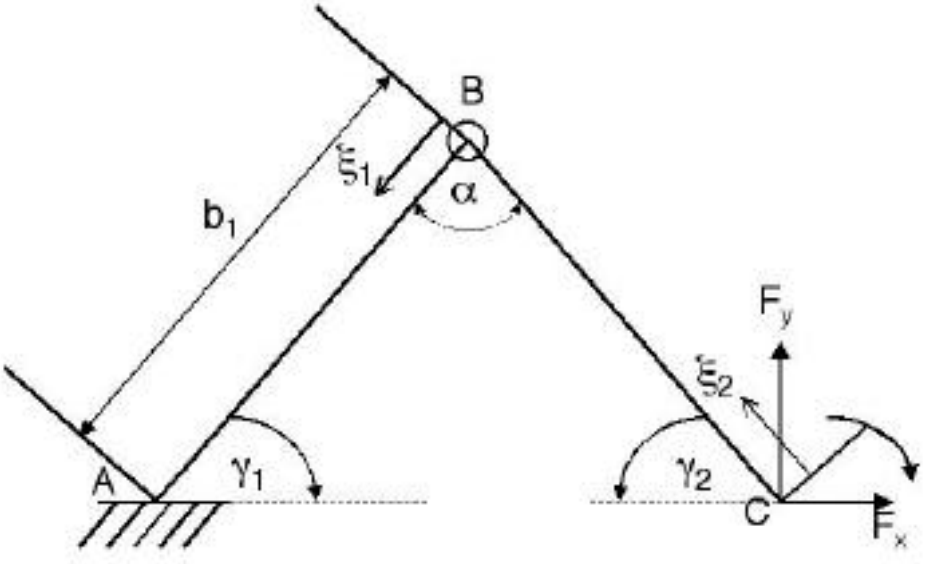

Figure 8. *Two-beam assembly of beams joined by a torsion spring at B.*

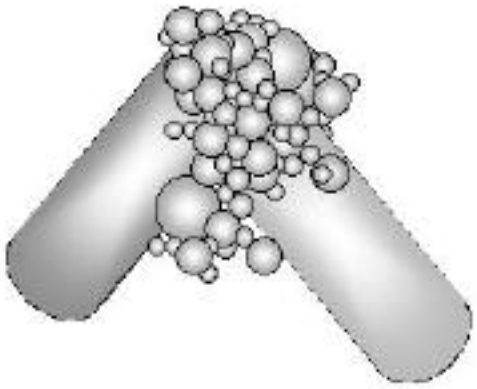

(a)

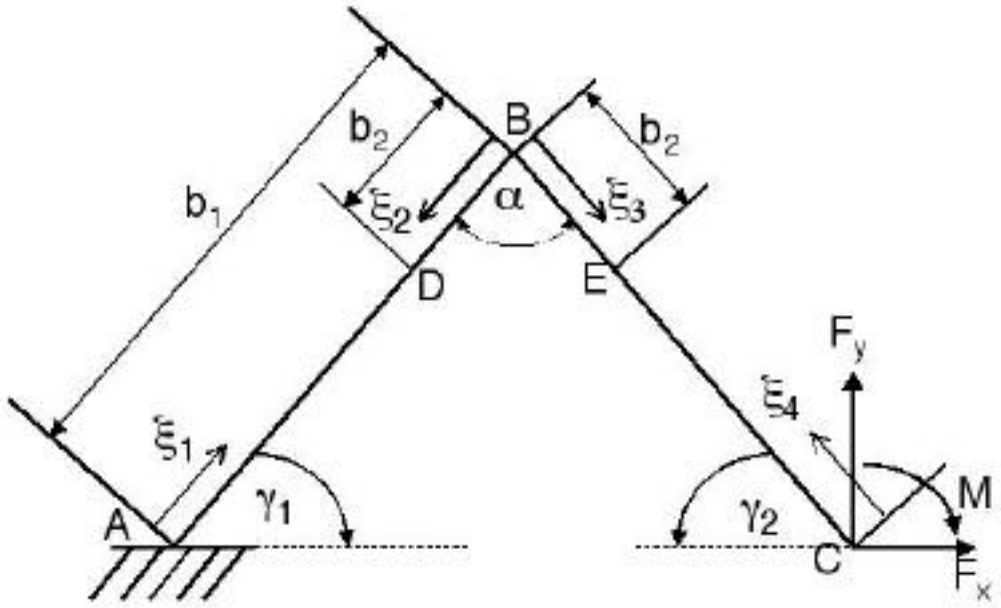

(b)

Figure 9. *A reduction of a physically realistic bond between fibers in a fiber/particle network to a 2D assembly (a), and notation for the two-beam assembly of rigidly joined beams, with each beam having a "compliant zone" of length b_2 (b)*

allows for solution of all internal displacements and moments. The normalized torsion spring constant is given by

$$\overline{K} = \frac{Kl}{EI} \tag{3}$$

where K is the torsion spring constant, l is the total beam length ($l=l_1+l_2$), and E and I are the usual modulus and moment of inertia.

For the compliant zone model pictured in Fig. 9, wherein lengths of the connected beams are assumed to have some stiffness other than the beam material, we establish a correspondence with the torsion spring model as

$$E_1 = \frac{2E(b_1-b_2)\left[\tan(\gamma)^2 A\left[E^2I^2b_1b_2 - K^2b_1^4 - 2EKb_1^2I(b_1-b_2)\right] - 12IKL(EI+Kb_1) - 3E^2I^3\right]}{\left(b_2IE + 2b_2b_1K - 2Kb_1^2\right)\left(6EI^2 + 2EA\tan(\gamma)^2 b_1^2I + 12b_1KI + AK\tan(\gamma)^2 b_1^3\right)} \tag{4}$$

$$E_2 = \frac{-2Eb_2\left[\tan(\gamma)^2 A\left[E^2I^2b_1b_2 - K^2b_1^4 - 2EKb_1^2I(b_1-b_2)\right] - 12IKb_1(EI+Kb_1) - 3E^2I^3\right]}{\left(b_2IE + Ib_1E + 2b_1b_2K\right)\left(6EI^2 + 2EA\tan(\gamma)^2 b_1^2I + 12b_1KI + AK\tan(\gamma)^2 b_1^3\right)} \tag{5}$$

where E_1 and E_2 are the moduli of the beam material and the material in the compliant zone, respectively. Thus, a reduction in modulus of a zone of connection is possible to implement either by placement of a torsion spring at the joint (Fig. 8) or by assumption of a compliant zone around the joint due to joining by perhaps an interconnecting, porous material (Fig. 9).

Investigation of the moduli and strength of the of networks reveals that the key element in a very significant range of structures is, in fact, the compliance of the bond, as illustrated by Fig. 10, showing the strong influence of joint compliance for both modulus and strength. Indeed, the model selected for the fiber strut (in this case, Timoshenko versus Euler beams) has little effect, even for short beams, and especially when compared with the properties of the joint. Thus, the connectivity of the network and the bond densities play a key role in assessing scale effects in simulation. Results for simple assemblies of connected beams are shown in Fig. 11. Because of the large effect of bond compliance, these degenerate networks illustrate the importance of scale in calculation of network modulus.

In light of the significance of bond type, we have recently [18] modeled 3D interconnects in fiber/particle networks. We characterize the interpenetration of fibers or particles as degree of intersect (d.o.i.), as shown in Figs. 12 and 13.

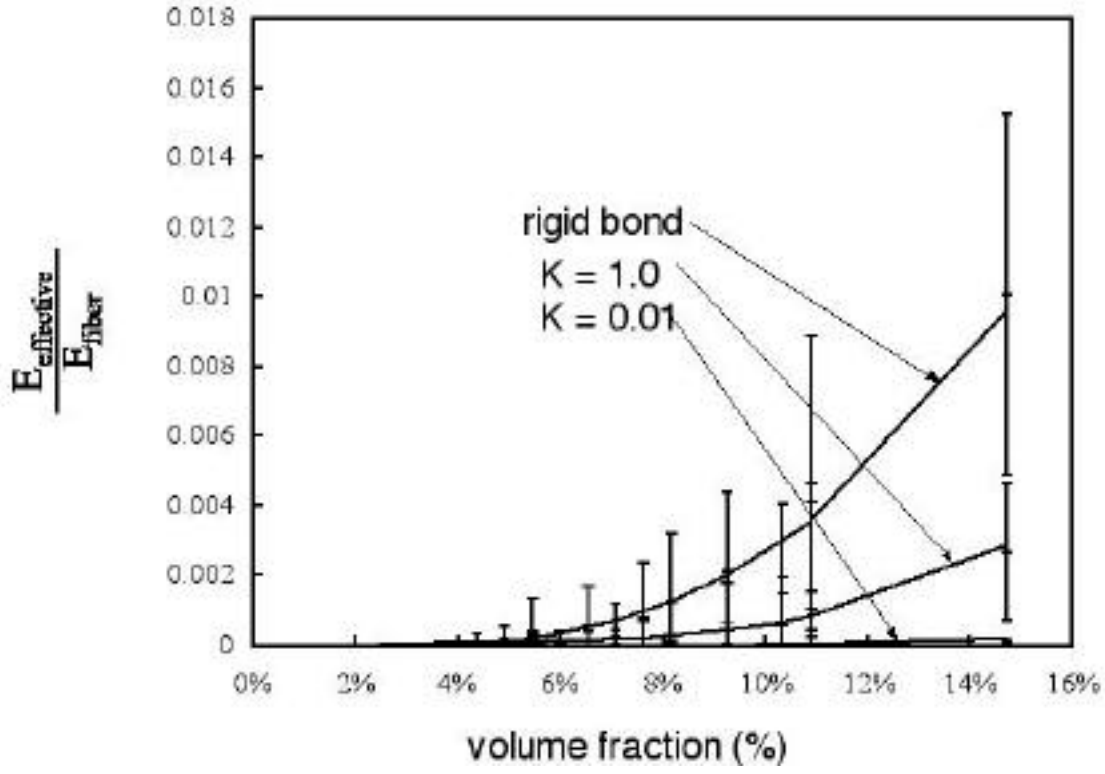

(a)

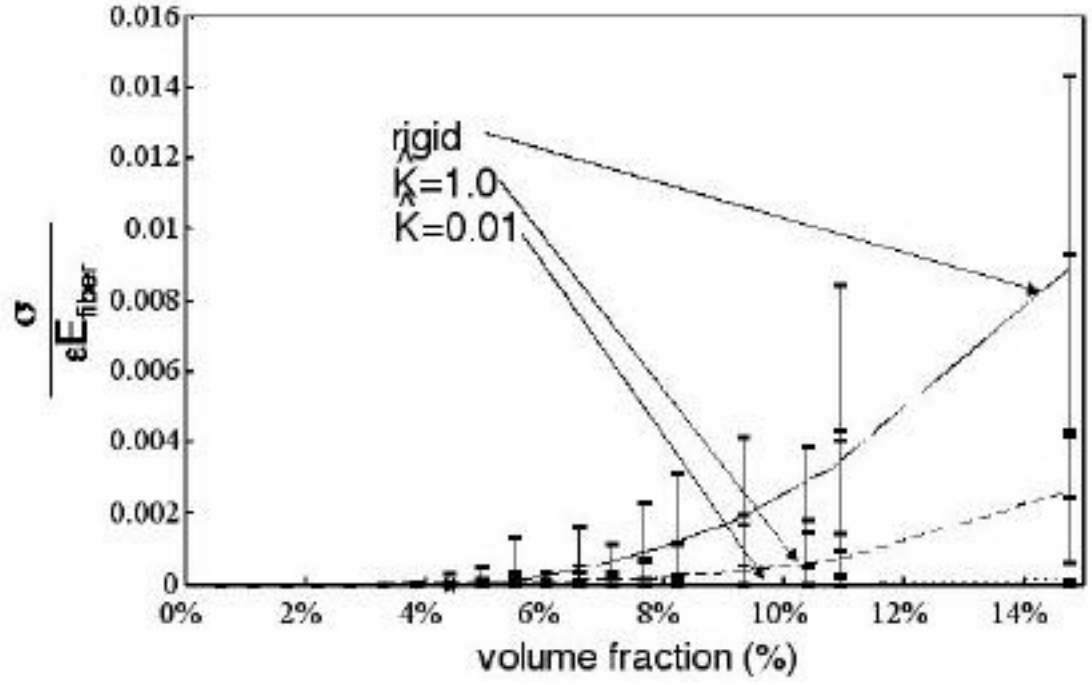

(b)

Figure 10. *Normalized effective moduli (a) and peak stress (b) for two normalized torsion spring constants. Plots were for networks comprised of fibers with uniform aspect ratio of 10, with representative cell edge length of* $l_c = 1.2$.

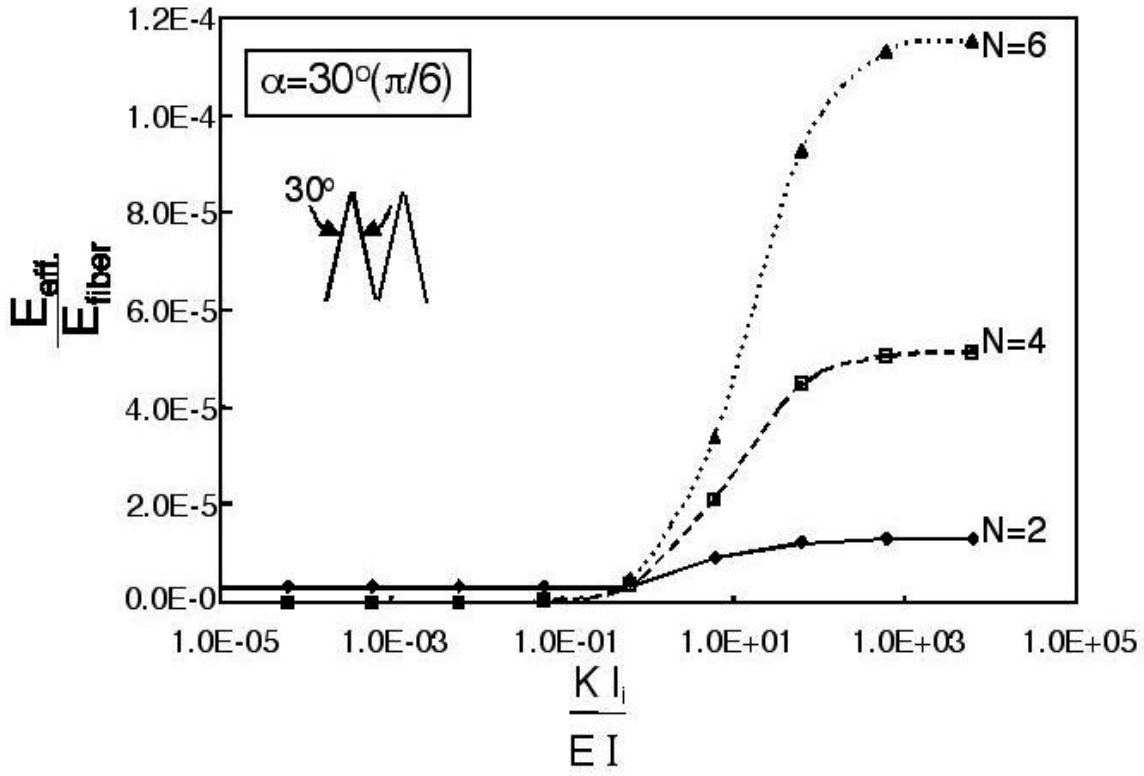

(a)

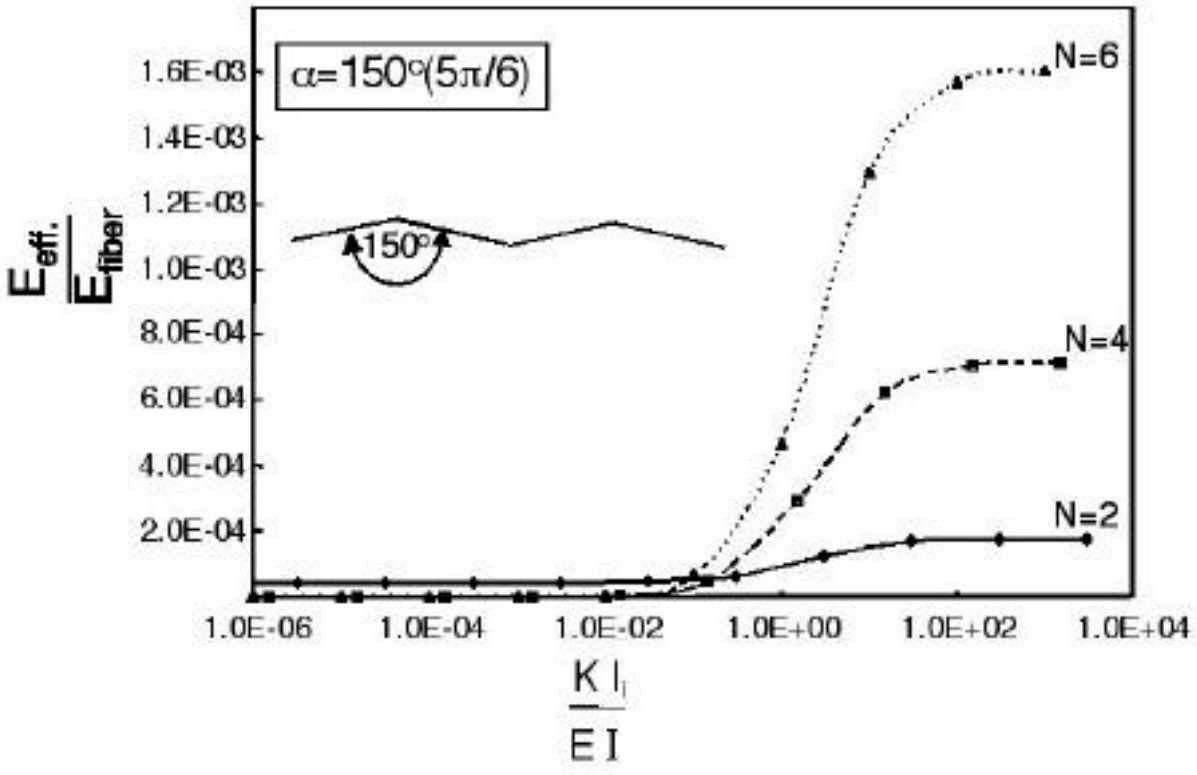

(b)

Figure 11. *Effective moduli (a) and maximum stresses (b) are given for a=30 and a=150 deg, for a range of torsion spring constants and a variable number of segments. (Four segments case is illustrated for both (a) and (b)).*

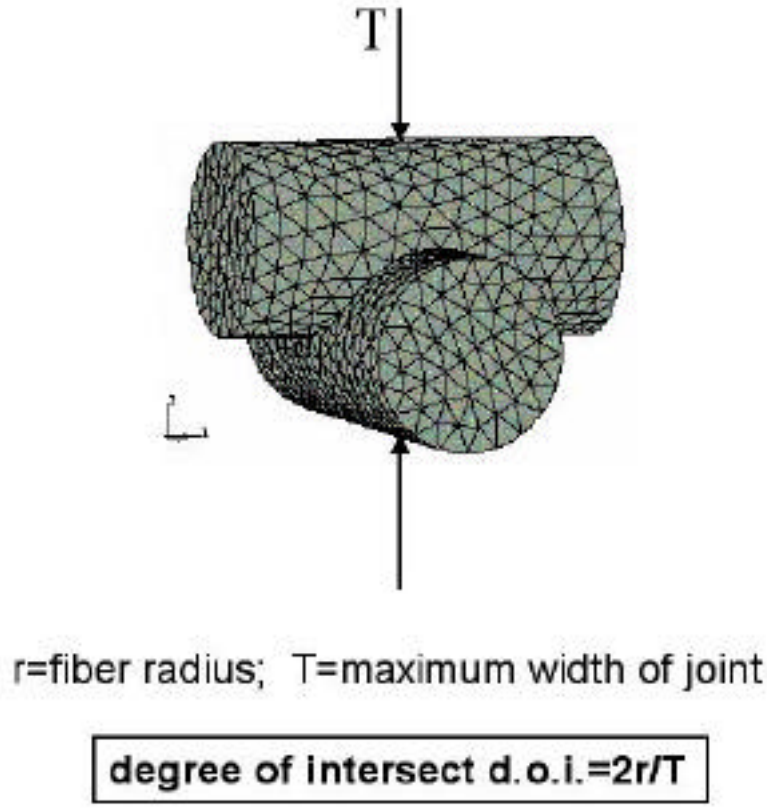

Figure 12. *Definition of the degree of intersect (d.o.i.).*

This type of interpenetration, however, has two major deficiencies: first, the stress singularity produced by the sharp interconnect line prevents reasonable calculation of maximum stress in the assembly in the linear elastic range, and second, volume (mass) conservation is violated when two fibers or particles are bonded to one another, if the displaced material is not redistributed. Addition of a smoothing fillet as in Fig. 14 remedies both deficiencies, smoothing the stress singularity and allowing modeling of menisci, similar to those occurring in real sintered or coated materials to redistribute mass (Fig. 15). Presently, we are investigating the importance of these types of physically realistic bonds in assessing local damage progression.

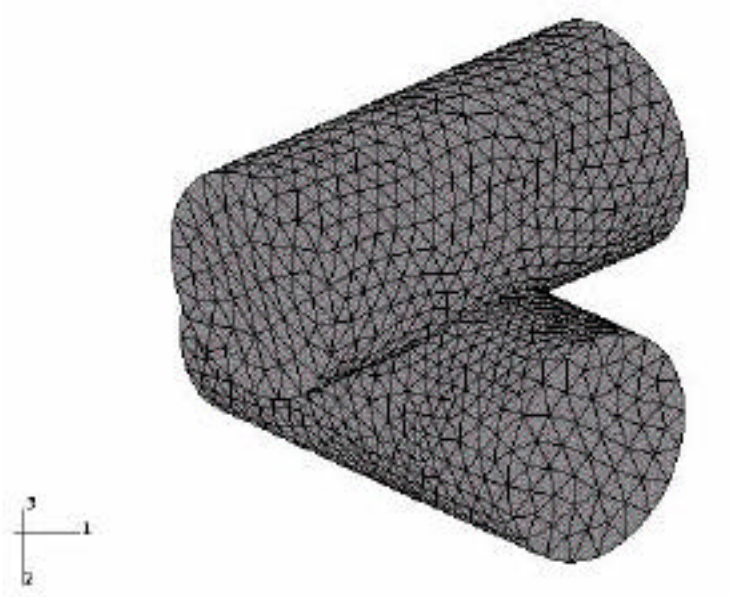

(a)

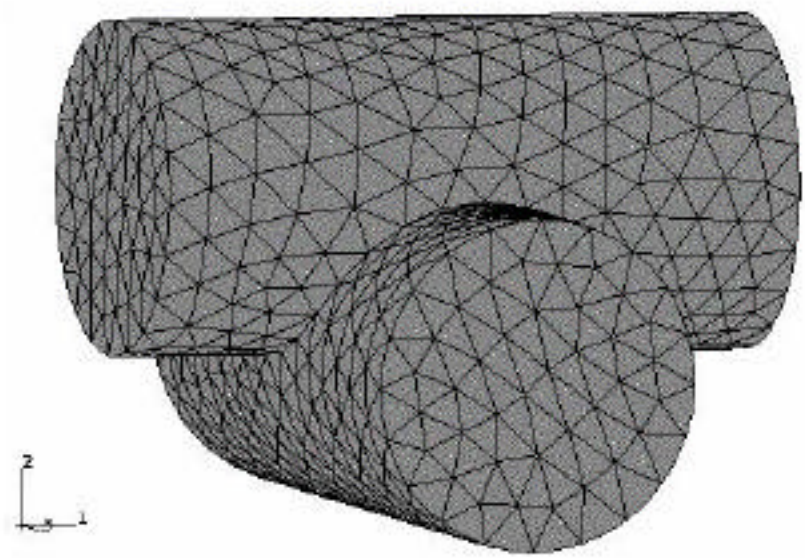

(b)

Figure 13. *3D modeling without fillet. Detail of the joint of a finite element model of two intersecting fibers with (a) d.o.i.=0.571 and (b) d.o.i.=0.667.*

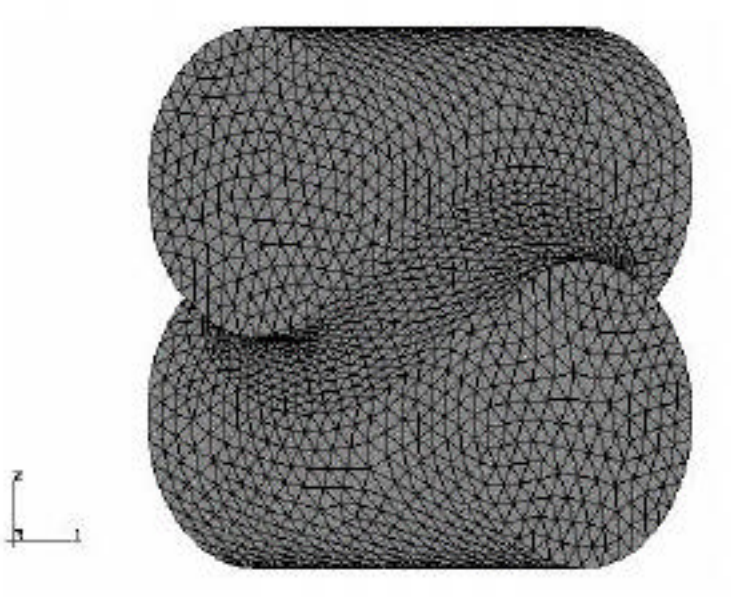

(a)

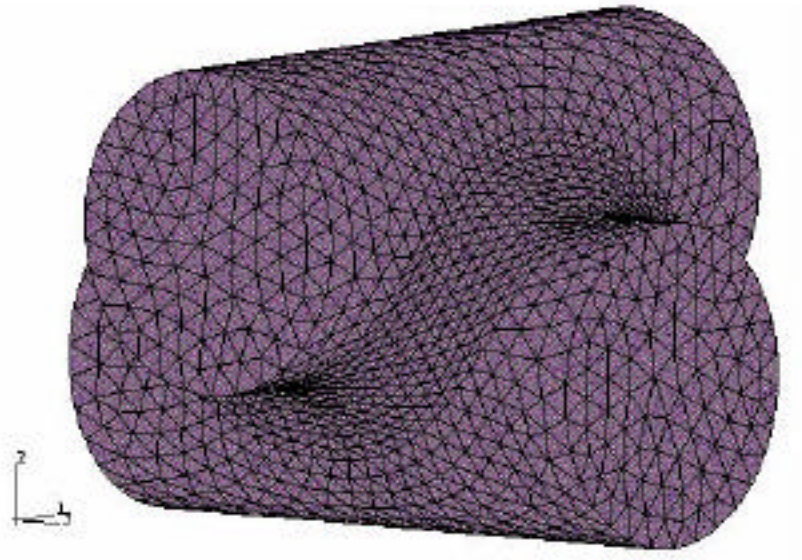

(b)

Figure 14. *3D modeling with fillet. Detail of the joint of a finite element model of two intersecting fibers with (a) d.o.i.=0.571 and (b) d.o.i.=0.667.*

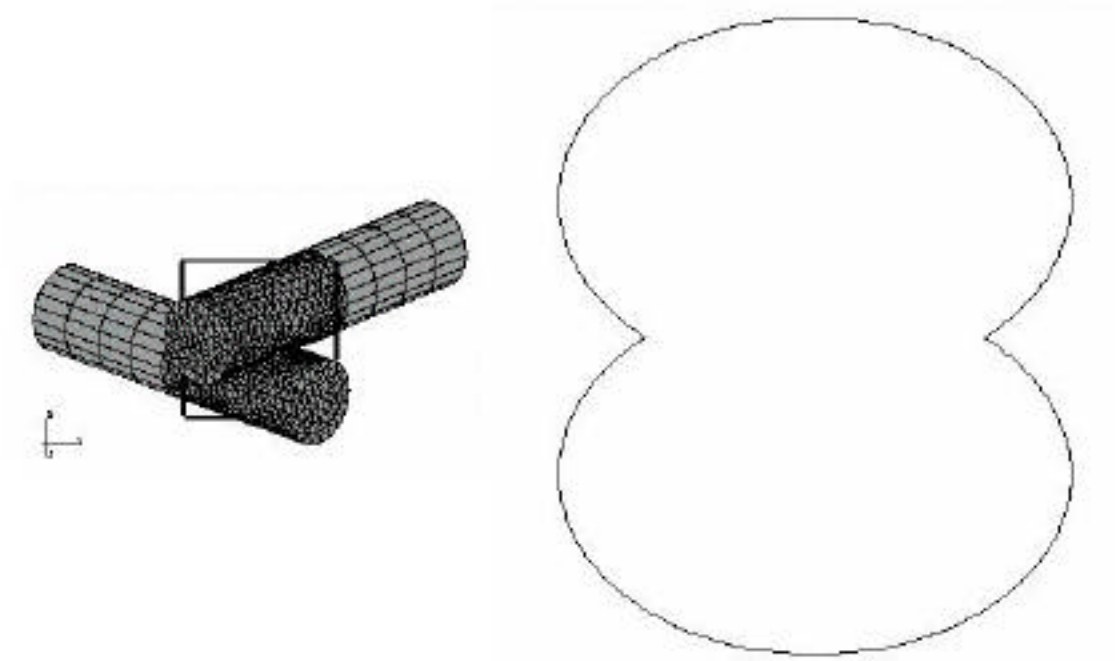

(a)

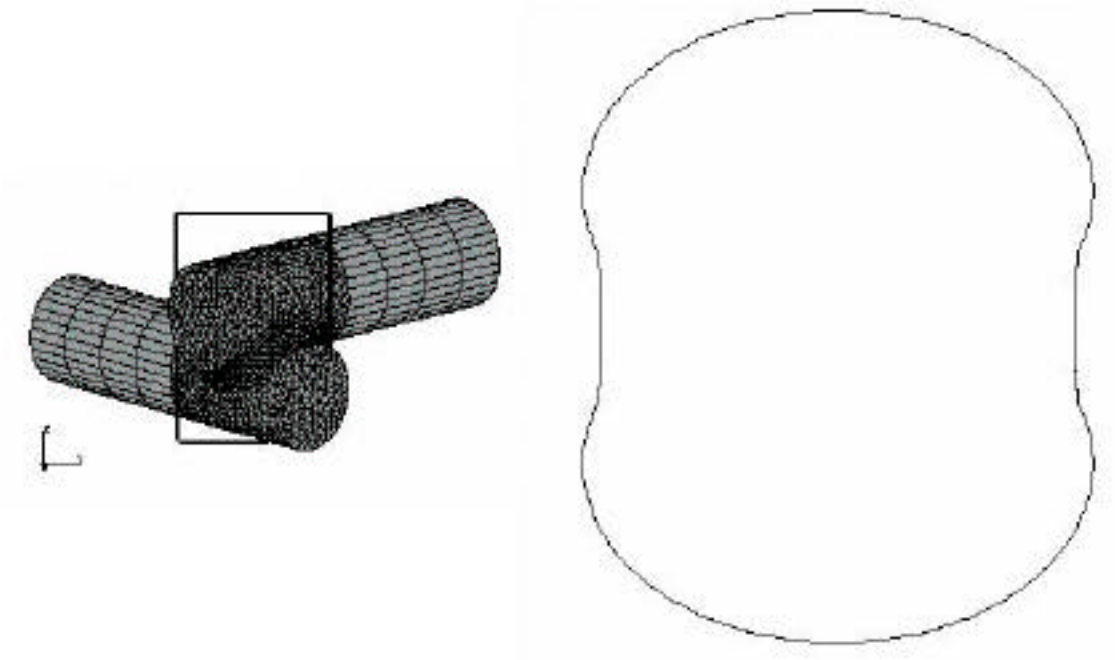

(b)

Figure 15. *Sections through the joints of two fibers intersecting with d.o.i.=0.571 for (a) a model without a fillet and (b) a model with a fillet included. The section in (b) shows that the sharp corners (and hence the stress singularities) are eliminated by the introduction of a fillet.*

4. Future Directions: Toward Improved Microstructural and Nanostructural Design

As the line between material and device continues to become blurred, investigation of the details of material connectivity and consideration of loads in multifunctional materials will become more critical, particularly at very small scales. As such, the classical approach of definition of an appropriate RVE will likely be supplanted by use of stochastic representation of small structures, in conjunction with FE or other numerical techniques for analysis of response. Coupling of microstructure and application are particularly important in this newer direction. In the electrochemical materials described here, the specific morphological changes and *in situ* loads significantly affect the way in which material geometry is specified. Nonetheless, investigation of a few key general phenomena, including bonding, scale and phase contrast using these models has shown potential application in a number of newer materials systems. A prominent goal is improved understanding of biomaterials, in both the evolutionary biology context, and in the context of improved understanding of damage progression in tissues.

5. Acknowledgements

This work was sponsored by the National Science Foundation through a PECASE grant, the U.S. Department of Energy through the Lawrence Berkeley Laboratories BATT program, and ONR and DARPA through the Synthetic Multifunctional Materials Program. The authors are grateful for the generous support of these sponsors.

List of Symbols

A	cross-sectional area
A_s	shear area
b_1	total length of each beam in compliant zone model
b_2	length of "compliant zone"
$d_{segment}$	diameter of a segment in a beam network
E	Young's modulus
E_1, E_2	Young's moduli of segments of compliant zone model
$E_{effective}$	effective Young's modulus of a beam assembly
F_1, F_2	axial force (subscript denotes end at which it is applied)
F_{AB}, F_{BC}	axial forces in members AB and BC of torsion spring model
F_{AD}, F_{DB},	axial forces in members AD and DB of compliant zone model
F_{BE}, F_{EC}	axial forces in members BF and BC of compliant zone model
F_{x1}, F_{x2}	applied force at point C in x-direction. Subscript 1 denotes compliant zone model and 2, the torsion spring model
F_{y1}, F_{y2}	applied force at point C in y-direction. Subscript 1 denotes compliant zone model and 2, the torsion spring model
G	shear modulus
I	second moment of area
K	torsion spring constant
K_1, K_2	torsion spring constant. Subscript denotes end at which spring is located
L	beam length
l_1, l_2	beam lengths
M_1, M_2	applied moment at point C. Subscript 1 denotes compliant zone model and 2, the torsion spring model
M_{AB}, M_{BC}	moment in members AB and BC of torsion spring model
M_{AD}, M_{DB}	moment in members AD and DB of compliant zone model
M_{BF}, M_{BC}	moment in members BF and BC of compliant zone model
Q_1, Q_2	bending moment (subscript denotes end at which it is applied)
S_1, S_2	shear force (subscript denotes end at which it is applied)
u	x-direction displacement
v	y-direction displacement
X_1, X_2	x-direction displacement of point C. Subscript 1 denotes compliant zone model and 2, the torsion spring model
Y_1, Y_2	y-direction displacement of point C. Subscript 1 denotes compliant zone model and 2, the torsion spring model
α_1, α_2	internal rotation between two beams (subscripts denote end)
ξ_1, ξ_2, ξ_3, ξ_4	local coordinates along beam segments of compliant zone and torsion spring models
α	angle between beams in two-beam assembly
γ_1, γ_2	angles between beams of two-beam assembly and x-axis

REFERENCES

[1] C.W. Wang, L. Berhan and A.M. Sastry: ASME Journal of Engineering Materials and Technology Vol.122 (2000), pp. 450-459.

[2] C.W. Wang and A.M. Sastry: ASME Journal of Engineering Materials and Technology Vol. 122 (2000), pp. 460-468.

[3] C. Wang, X. Cheng, A.M. Sastry and S.B. Choi: ASME Journal of Engineering Materials and Technology Vol. 121 (1999), pp. 503-513.

[4] X. Cheng, C. Wang, A.M. Sastry and S.B. Choi: ASME Journal of Engineering Materials and Technology Vol. 121 (1999), pp. 514-523.

[5] A.M. Sastry, X. Cheng and C. W. Wang: Journal of Thermoplastic Composite Materials Vol. 11 (1998), pp. 288-296.

[6] X. Cheng and A.M. Sastry: Mechanics of Materials Vol. 31 (1999), pp. 765-786.

[7] X. Cheng, A.M. Sastry and B.E. Layton: ASME Journal of Engineering Materials and Technology Vol. 123 (2001), pp. 12-19.

[8] A.M. Sastry, S.B. Choi and X. Cheng: ASME Journal of Engineering Materials and Technology Vol. 120 (1998), pp. 280-283.

[9] S.R. Broadbent and J.M. Hammersly: Proceedings. Cambridge Philosophical Society Vol. 53 (1957), pp. 629-641.

[10] O. Kallmes and H. Corte: TAPPI Vol. 43 (1960), pp. 737-752.

[11] H. Corte: Structure, Solid Mechanics and Engineering Design, the Proceedings of the Southampton 1969 Civil Engineering Materials Conference, Part1, Edited by Te'eni, M., Wiley-Interscience, 1971, pp.314-355.

[12] S. Kirkpatrick: Reviews of Modern Physics Vol. 45 (1973), pp. 574-588.

[13] G.E. Pike and C.H. Seager: Physical Review B Vol. 10 (1974), pp. 1421-1434.

[14] C.H. Seager and G.E. Pike: Physical Review B Vol. 10 (1974), pp. 1435-1446.

[15] I. Balberg and N. Binenbaum: Physical Review B Vol. 28 (1983), pp. 3799-3812.

[16] I. Balberg and N. Binenbaum: Physical Review Letters Vol. 52 (1984), pp. 1465-1468.

[17] R.E. Meredith and C.W. Tobias: Advances in Electrochemistry and Electrochemical Engineering (Interscience, New York 1962) pp. 15–47.

[18] L. Berhan, C.-W. Wang and A.M Sastry, manuscript in preparation, 2001.